

*“A global dataset of  $\delta^{13}\text{C}\text{-CH}_4$  source signatures and associated uncertainties (1998–2022), with a sensitivity analysis to support isotopic inversions”*

*By Tapin et al. (essd-2025-668)*

Submitted to Earth System Science Data (ESSD)

**Legend:**

**Reviewer comments** are reproduced in dark blue.

**Author responses** are in black.

**Manuscript changes** are shown in purple italics, with line numbers referring to the revised manuscript.

## Response to Reviewer 1

### General response

We sincerely thank Reviewer 1 for the careful and constructive evaluation of our manuscript, and for the strong support expressed for publication. We are grateful for the detailed list of references provided, several of which we had not yet incorporated, and for the helpful suggestions concerning latitudinal variability, the freshwater and geological sources, the chlorine and stratospheric sinks, and tropical measurement programs. We have addressed all comments individually below. The reviewer’s suggestions have led to substantive improvements, in particular to the discussion of latitudinal  $\text{C}_3/\text{C}_4$  gradients, the explicit acknowledgement of large uncertainties in freshwater and geological emission estimates, the expanded treatment of the chlorine and stratospheric sinks, and the inclusion of recent tropical measurement campaigns in our reference list. All line numbers in our responses refer to the revised manuscript.

### Response to general comments

#### G1. Lack of tropical data and latitudinal variation ( $\text{C}_3/\text{C}_4$ plants in agriculture, wetlands, and biomass burning)

**Reviewer comment:** “There are many factors driving strong latitudinal gradients. In particular,  $\text{C}_4$  plants, which pre-concentrate and thus accept more  $^{13}\text{C}$  in photosynthesis, are dominant in the tropical grasslands and wetlands (e.g. papyrus), while  $\text{C}_3$  rules in the boreal realm. Also in the sinks, in the Brewer-Dobson circulation the polar vortex delivers low mixing ratio, highly  $^{13}\text{C}$  rich methane, while in the tropical troposphere the upward loss to stratosphere is of high mixing ratio  $^{12}\text{C}$  rich methane.”

**Response:** We fully agree that latitudinal gradients arising from the  $\text{C}_3/\text{C}_4$  plant distribution and from stratospheric transport processes deserve more explicit discussion. We have substantially expanded our treatment of these issues in three places in the revised manuscript.

First, in Section 2.3 (uncertainty assessment) we now explicitly state that propagated uncertainties carry a latitudinal dimension driven by the C<sub>3</sub>/C<sub>4</sub> distribution and by stratospheric transport. Second, in Section 4.1.1 (spatial patterns) we expanded the discussion of all three affected sectors (AGW, BB, WET) to highlight the role of C<sub>3</sub> versus C<sub>4</sub> vegetation, citing the additional references suggested by the reviewer. Third, in Section 4.1.3 we added a dedicated paragraph on the latitudinal structure of propagated uncertainties.

**Manuscript change (Section 4.1.1, AGW bullet, L 416–419):** *“Livestock signatures show notable regional variability: tropical regions tend to be more enriched (heavier than –60‰) due to C<sub>4</sub>-dominated forage, while temperate extensive grazing systems on C<sub>3</sub> grasslands yield more depleted values. However, intensive dairy systems in the northern hemisphere, fed largely on C<sub>4</sub> maize silage, can also produce relatively enriched signatures (Chang et al., 2019).”*

**Manuscript change (Section 4.1.1, BB bullet, L 420–424):** *“Isotopic gradients are primarily latitudinal, driven by the distribution of C<sub>3</sub> and C<sub>4</sub> plants. Tropical and subtropical regions dominated by C<sub>4</sub> vegetation exhibit more enriched values, while boreal regions show more depleted signatures (Still et al., 2003; Randerson et al., 2012; Lan et al., 2021a). Within the tropics, grass fires burning C<sub>4</sub> vegetation tend to produce more enriched δ<sup>13</sup>C-CH<sub>4</sub> than bush and tree fires, which involve predominantly C<sub>3</sub> biomass (Barker et al., 2020; France et al., 2022).”*

**Manuscript change (Section 4.1.1, WET bullet, L 425–427):** *“Generally depleted values (–50 to –70‰) are observed, with more depleted signatures in high-latitude and boreal wetlands, and relatively enriched ones in tropical wetlands, where C<sub>4</sub> aquatic vegetation such as papyrus contribute to isotopically heavier signatures (Ganesan et al., 2018; Oh et al., 2022; Nisbet et al., 2021; France et al., 2022).”*

**Manuscript change (Section 4.1.3, latitudinal structure paragraph, L 540–545):** *“Beyond sectoral aggregation, the propagated uncertainties also exhibit a latitudinal structure. The distribution of C<sub>3</sub> and C<sub>4</sub> plants drives systematic gradients in isotopic signatures across the WET, BB, and AGW sectors: tropical regions, dominated by C<sub>4</sub> vegetation, tend to produce more enriched δ<sup>13</sup>C-CH<sub>4</sub> signatures, while boreal and temperate regions, where C<sub>3</sub> plants prevail, yield more depleted values (Still et al., 2003; Chang et al., 2019; France et al., 2022; Nisbet et al., 2021).”*

Regarding the lack of tropical isotopic measurements, we now emphasise this issue more strongly in Sections 4.1.3 and 4.1.4 and refer explicitly to the recent MOYA and ZWAMPS campaigns (France et al., 2022; Nisbet et al., 2021; Shaw et al., 2022; Barker et al., 2020). The tropical wetland source signatures of  $-59.0 \pm 1.3\text{‰}$  (Bolivian Amazonia, France et al., 2022) and  $-59.3 \pm 2.0\text{‰}$  (Zambia/Bolivia composite, Nisbet et al., 2021) are now discussed in Section 4.1.4, where we note their consistency with the tropical wetland values used in our maps and acknowledge that these recent airborne measurements have not yet been assimilated into process-based wetland isotope models.

## G2. Weighting given to freshwater sources

**Reviewer comment:** “Freshwater systems. I’m very sceptical here, but I realise this is a long-running puzzle and in this paper I think the best approach is simply to say briefly that fluxes are very uncertain. The re-scaling by one-third maybe should get a further note here, in addition to the reference to Saunois et al 2025. Note for example the Shaw et al. paper, which is one of the very few to study the Congo freshwater and wetlands.”

**Response:** We agree with the reviewer’s scepticism and adopt the suggested approach. The aim of our work is not to defend a particular freshwater flux estimate, but rather to be consistent with the Global Methane Budget framework while clearly flagging that this estimate is highly uncertain. We have expanded the description of freshwater fluxes in Section 3.1.2 to explicitly state the large uncertainties surrounding these estimates and the limitations of the one-third rescaling, and we now cite Shaw et al. (2022), which we had inadvertently overlooked.

**Manuscript change (Section 3.1.2, L 277–282):** *“Freshwater systems: Emissions from lakes and reservoirs are based on the CH<sub>4</sub> flux maps by Stavert et al. (2022). Initial global emissions are estimated at 95 Tg yr<sup>-1</sup>, reduced to 73 Tg yr<sup>-1</sup> after ice-cover corrections. Following Martinez et al. (2024), emissions are further rescaled by a factor of one-third, resulting in a global total of 53 Tg yr<sup>-1</sup> (Saunois et al., 2025). We acknowledge that freshwater flux estimates remain subject to large uncertainties, arising from poorly mapped inland water extent, complex emission pathways, and spatial variability in methanotrophy (e.g., Van Bergen et al., 2019; Lauerwald et al., 2023; Shaw et al., 2022). These uncertainties are further discussed in Sect. 4.2.2.”*

We therefore retain the GMB freshwater value as a working assumption (rather than an established constraint) and emphasise in Section 4.3.2 that omitting freshwaters entirely would bias regional attribution, while including them as a separately optimised category remains premature given the available observational constraints.

## G3. Weighting given to geological sources

**Reviewer comment:** “Petrenko et al have presented convincing evidence that the Etiope et al estimate of geological emissions is much too high, and I suspect even the downsized 21.1 Tg guess in Table 1 is still high. (...) I strongly suspect this 23 Tg/yr figure is too high.”

**Response:** We agree with the reviewer that the geological emission estimate of ~21–23 Tg yr<sup>-1</sup> is contested by the ice-core constraints from Petrenko et al. (2017) and other related work. In our framework, we adopted the geological flux from the Global Methane Budget (Martinez et al., 2024) for consistency across our reference simulations, and we did not perform a sensitivity test on this value. To address the reviewer’s concern, we have added an explicit caveat in Section 3.1.2 stating that the current value follows the GMB framework but that ice-core-based constraints suggest substantially lower pre-industrial geological emissions. We note that since this value is held constant in our reference simulations and contributes only a small fraction of the FFG sector flux, the impact on the modeled δ<sup>13</sup>C-CH<sub>4</sub> signal is limited; however, the reviewer’s point underscores a structural uncertainty that should be addressed in future inversion studies.

**Manuscript change (Section 3.1.2, L 285–290):** *“Geological methane: Geological emissions use the gridded climatology from Etiope et al. (2019), rescaled to a total global flux of 21 Tg CH<sub>4</sub> yr<sup>-1</sup> by Martinez et al. (2024). Offshore geological emissions, including marine seepage, are excluded to avoid double counting. We note that geological emission estimates remain uncertain; ice core-based constraints suggest that pre-industrial geological emissions may have been substantially lower (Petrenko et al., 2017), though the current value follows the Global Methane Budget framework (Martinez et al., 2024) for consistency with the broader modeling setup.”*

#### G4. The chlorine sink

**Reviewer comment:** *“The chlorine sink is small for methane in Tg but disproportionately large in its leverage on  $\delta^{13}\text{C}$ ... this is an important factor as the sink is still poorly quantified. It probably needs a somewhat longer discussion. Maybe also refer to Allen et al. 2007.”*

**Response:** We agree that the Cl sink, while small in mass terms, has disproportionate isotopic leverage and merits a more substantial discussion. We have added a dedicated paragraph in Section 4.2.3 covering: (i) the magnitude of the tropospheric Cl sink based on the most recent estimates (~1–3% of total CH<sub>4</sub> oxidation; Hossaini et al., 2016; Sherwen et al., 2016; Gromov et al., 2018; Wang et al., 2021; Saunio et al., 2025), with explicit reference to Allan et al. (2007) for context on earlier estimates; (ii) the strong KIE of the Cl reaction ( $\approx 1.066$ ), more than an order of magnitude larger than that of OH; and (iii) a quantitative summary of the Thanwerdas et al. (2022b) sensitivity analysis, which used the same ClF–LMDz–SACS framework as ours and reported a near-linear sensitivity of +11.7 Tg CH<sub>4</sub> yr<sup>-1</sup> and –1.0‰ in the globally averaged source signature per 1000 molec. cm<sup>-3</sup> increase in mean tropospheric Cl, with stratospheric Cl alone contributing a ~0.30‰ surface enrichment via stratosphere–troposphere exchange.

We explain that we did not repeat a Cl sensitivity experiment because it would essentially duplicate Thanwerdas et al. (2022b) within the same model framework, but we acknowledge that uncertainties in Cl concentrations remain a leading factor limiting isotope-based source partitioning, in agreement with Basu et al. (2022) and Röckmann et al. (2024b). We also added a note in Section 4.4 on emerging evidence for previously unaccounted-for Cl sources, notably photocatalytic release from mineral dust–sea spray aerosol (van Herpen et al., 2023; Röckmann et al., 2024a), as a relevant target for future inversion setups.

**Manuscript change (Section 4.2.3, chemistry paragraph, L 858–873):** *“The Cl sink accounts for a small fraction of total CH<sub>4</sub> oxidation. Recent estimates converge on a tropospheric contribution of ~1–3% of the total chemical sink (Hossaini et al., 2016; Sherwen et al., 2016; Gromov et al., 2018; Wang et al., 2021), with the latest Global Methane Budget reporting a climatological tropospheric Cl sink of 6 [1–13] Tg CH<sub>4</sub> yr<sup>-1</sup> (Saunio et al., 2025), substantially smaller and better constrained than earlier estimates (Allan et al., 2007). Despite this small magnitude, the Cl reaction carries an exceptionally large kinetic isotope effect (KIE  $\approx 1.066$  at 298 K; Saueressig et al., 1995), more than an order of magnitude larger than that of OH, so even modest uncertainties in Cl concentrations translate into substantial shifts in modeled  $\delta^{13}\text{C}\text{-CH}_4$  (see Table 2). Basu et al. (2022) further identified the combined uncertainty in fractionation (OH-KIE and Cl contribution) as the single most*

*important factor limiting isotope-based source partitioning at the global scale (Röckmann et al., 2024b). Thanwerdas et al. (2022b) quantified this influence within the same CIF-LMDz-SACS framework used here, and reported a near-linear sensitivity of +11.7 Tg CH<sub>4</sub> yr<sup>-1</sup> and -1.0 ‰ in the globally averaged source signature per 1000 molec. cm<sup>-3</sup> increase in mean tropospheric Cl, with stratospheric Cl alone contributing a ~ 0.30 ‰ surface enrichment via stratosphere–troposphere exchange and modifying the δ<sup>13</sup>C-CH<sub>4</sub> seasonal cycle amplitude by up to 10–20% depending on latitude. Because our configuration adopts the Cl field from Wang et al. (2021), consistent with the most recent tropospheric chlorine chemistry, the Cl-related uncertainty in our simulations is bounded by the ranges quantified in Thanwerdas et al. (2022b), which are of the same order of magnitude as the OH-KIE sensitivity reported in Table 6. A dedicated Cl sensitivity experiment was therefore not repeated here to avoid duplicating a recent and comprehensive analysis with the same model.”*

## G5. The stratospheric sink

**Reviewer comment:** “I am concerned by two problems – 1) the Cl sink with its large isotopic leverage and 2) the stratospheric sink. Both of these seem poorly understood and with high uncertainty. (...) Table 6 – Chemistry – mention the stratospheric sink?”

**Response:** We agree that the stratospheric sink merits more explicit discussion. In our model, methane oxidation in the stratosphere is represented by reactions with OH, O(<sup>1</sup>D) and Cl, with 3-D oxidant fields prescribed (Section 3.1.4, Table 2). The stratospheric component of the Cl sink is therefore implicitly included in the simulations. To make this clearer, we have added a footnote to Table 6 stating that the Cl sink is not perturbed independently in the sensitivity ensemble, with reference to the Thanwerdas et al. (2022b) results that quantify both tropospheric and stratospheric Cl contributions in the same framework. We have also expanded the discussion in Section 4.2.3 (see also G4 above) to explicitly address the stratospheric Cl contribution and its impact on the surface δ<sup>13</sup>C-CH<sub>4</sub> signal via stratosphere–troposphere exchange.

**Manuscript change (Section 4.4, transport paragraph, L 1029–1038):** “A second priority concerns atmospheric transport and chemistry, which were not perturbed in our sensitivity ensemble. All simulations were performed with LMDz at a single resolution (Sect. 3.1.1), and the TransCom-CH<sub>4</sub> intercomparison (Patra et al., 2011) showed that modeled CH<sub>4</sub> budgets are sensitive to troposphere–stratosphere exchange rates and to vertical grid structure, with CH<sub>4</sub> lifetimes spanning 9.50–10.27 yr across 12 CTMs using identical OH fields. For δ<sup>13</sup>C-CH<sub>4</sub>, vertical transport additionally controls the rate at which <sup>13</sup>C-enriched stratospheric air re-enters the troposphere via the Brewer–Dobson circulation, as well as the vertical distribution of the Cl sink and its strong fractionation (Butchart, 2014; Thanwerdas et al., 2022b).”

## Response to specific comments

### L23 – Updated atmospheric CH<sub>4</sub> mole fraction

**Reviewer comment:** “1930 in 2024 – maybe cite NOAA (Lan et al. 2026) for end 2025.”

**Response:** We have updated the value to reflect the most recent NOAA observations and now cite Lan et al. (2026).

**Manuscript change - L21:** “...to reach 1946 ppb in November 2025 (Forster et al., 2023b; Lan et al., 2026).”

### L25 – Atmospheric lifetime

**Reviewer comment:** “Maybe distinguish perturbation life (12 yr, as cited in IPCC) from burden/flux life of 9 yr.”

**Response:** Thank you for this useful clarification. We have rephrased the sentence to explicitly distinguish the two timescales.

**Manuscript change - L24-25:** “Its relatively short atmospheric lifetime (about 9 years for the burden; Prather et al., 2012, and approximately 12 years for the perturbation lifetime, Forster et al. 2023b)...”

### L33 – Long reference list

**Reviewer comment:** “Maybe add Ciais et al. 2026, Fujita et al. 2025, Riddell-Young et al. 2025, and switch Nisbet 2019 to 2023.”

**Response:** We have added Ciais et al. (2026), Fujita et al. (2025b), and Riddell-Young et al. (2025) to the reference list at this location, and we have updated the citation of Nisbet et al. to the 2023 version. The full reference list at L33 in the revised manuscript now includes the original references plus these additions.

### L36 – Biomass burning

**Reviewer comment:** “Add biomass burning (both natural and anthropogenic).”

**Response:** We have updated the sentence to explicitly mention biomass and biofuel burning as both natural and anthropogenic sources.

**Manuscript change - L37-39:** “Methane emissions have both natural (around 200 Tg CH<sub>4</sub> yr<sup>-1</sup>, e.g., wetlands, freshwaters, geological sources, natural wildfires) and anthropogenic origins (around 320 Tg CH<sub>4</sub> yr<sup>-1</sup>, e.g., agriculture, fossil fuel, waste, and anthropogenic biomass and biofuel burning).”

### L64–66 / L271 – Geological emissions

**Reviewer comment:** “See also Line 270, and Table 1 FFG segment... Petrenko et al have presented convincing evidence that the Etiope et al estimate of geological emissions is much too high, and I suspect even the downsized 21.1 Tg guess in Table 1 is still high.”

**Response:** Addressed in the response to general comment G3 above. We have added a caveat in Section 3.1.2 referring to Petrenko et al. (2017) and acknowledging that the GMB-aligned value may overestimate geological emissions.

#### L82 – Reference to Fujita et al. 2025

**Reviewer comment:** “Also see Fujita et al 2025.”

**Response:** We have added a citation to Fujita et al. (2025b) in the discussion of multi-isotopic constraints on fossil methane emissions I33.

#### L227 – Sub-sector variability and latitudinal uncertainty

**Reviewer comment:** “Sub sector uncertainty and aggregation. This is interesting, but perhaps there should also be a brief discussion of latitudinal uncertainty... there are many factors driving strong latitudinal gradients.”

**Response:** We have addressed this point in detail (see G1). In addition to the spatial-pattern paragraphs in Section 4.1.1, we added a dedicated paragraph in Section 4.1.3 on the latitudinal structure of propagated uncertainties, and a closing sentence in Section 2.3 that anticipates this discussion.

**Manuscript change - L236-239:** *“In summary, this framework provides consistent tools to estimate sectoral  $\delta^{13}\text{C}\text{-CH}_4$  uncertainties, combining sub-sector variability and aggregation effects. Beyond sectoral aggregation, isotopic uncertainties also carry a latitudinal dimension, driven notably by the distribution of  $\text{C}_3$  and  $\text{C}_4$  plants across source sectors and by stratospheric transport processes; these spatial gradients are discussed further in Sect. 4.1.1.”*

#### L265 – Freshwater systems

**Reviewer comment:** See general comment G2.

**Response:** Addressed in the response to general comment G2 above. We have expanded the discussion of freshwater uncertainties in Section 3.1.2 and added a reference to Shaw et al. (2022).

#### L285 – Hydroxyl

**Reviewer comment:** “See Morgenstern et al. 2025, and Ciais et al. 2026.”

**Response:** We have added these references in Section 4.2.3, where we discuss the temporal evolution of tropospheric oxidative capacity and its implications for recent  $\text{CH}_4$  trends.

**Manuscript change - L825-829:** *“Recent studies further suggest that tropospheric oxidative capacity is itself evolving over time: Morgenstern et al. (2025) infer an increasing global OH abundance from radiocarbon monoxide ( $^{14}\text{CO}$ ) observations, with implications for the interpretation of recent  $\text{CH}_4$  trends (Ciais et al., 2026; Nisbet and Manning, 2026).”*

#### L292 / Table 2 – Chlorine sink

**Reviewer comment:** See general comment G4.

**Response:** Addressed in the response to general comment G4 above. We have expanded the CI-sink discussion in Section 4.2.3 and added Allan et al. (2007) to the reference list.

#### L394–397 / Fig. 1 – Latitudinal gradient of C<sub>3</sub> and C<sub>4</sub> plants

**Reviewer comment:** “Ganesan et al. is mentioned elsewhere (L482) in the paper but could be cited here too. Also see France et al. 2022, and Nisbet et al (MOYA) 2022. The C<sub>3</sub>/C<sub>4</sub> gradient affects: 1) wetland emissions – equatorial wetlands are papyrus rich, while outer tropics have more reeds (C<sub>3</sub>/C<sub>4</sub>) and boreal wetlands have almost no C<sub>4</sub> plants. 2) agricultural emissions – ruminant grazers eat grasses in the tropics that are mostly C<sub>4</sub>, but in the drier outer tropics cattle and antelope are often browsers, on C<sub>3</sub> trees. 3) biomass burns – tropical grass fires are C<sub>4</sub> rich but tropical bushes and tree fires are C<sub>3</sub>, so methane given off by incomplete combustion is somewhat less heavy. Boreal forest fires are C<sub>3</sub>. See Barker et al. 2020.”

**Response:** We thank the reviewer for this very detailed comment, which has helped substantially improve the spatial pattern discussion. We have integrated all three points (wetland, agricultural, biomass burning) into the bullet list of Section 4.1.1, with the appropriate citations. The corresponding manuscript changes are shown in our response to general comment G1 (AGW, BB and WET bullets).

#### L436 – AGW signature regional variability

**Reviewer comment:** “AGW signature is regionally very variable. In the tropics, heavier than –60‰. In the populated northern hemisphere, breath of grassland animals (mostly beef) is probably lighter than –60‰ but intensive livestock (especially dairy) are fed C<sub>4</sub> maize and their breath can be quite heavy.”

**Response:** We added a sentence to the AGW bullet in Section 4.1.1 reflecting this variability (see manuscript change in our response to G1, AGW bullet, L 416–419).

#### L482 / L501 – Lack of tropical measurements

**Reviewer comment:** “Emphasise the lack of tropical measurement?”

**Response:** We have strengthened this point in two places. In Section 4.1.3 (propagated uncertainty paragraph for WET), we now explicitly state that “Tropical wetlands in particular remain under-sampled, despite representing a dominant fraction of global wetland CH<sub>4</sub> emissions (France et al., 2021, 2022)”, and similarly for BB (“tropical fire-dominated regions being particularly under-represented in isotopic measurement databases”, citing Nisbet et al., 2021). In Section 4.1.4, we list “Uneven geographic coverage” as the first systematic bias inherited from observational databases, and explicitly note that recent tropical measurement programs (France et al., 2022; Nisbet et al., 2021; Shaw et al., 2022) have not yet been integrated into the maps.

#### L523 – Aggregation uncertainty for WET

**Reviewer comment:** “No aggregation uncertainty stated, but actually the aggregation involves aggregating different components of low latitude and high latitude results.”

**Response:** We agree that this point deserves clarification. Although our aggregation uncertainty  $\sigma_{agg}$ , defined as the variability across emission inventories used for flux-weighting, is null for WET because we use a single wetland flux dataset, the latitudinal contrast between tropical and boreal wetlands generates substantial isotopic variability that is captured by the propagated uncertainty  $\sigma_{prop}$ . We have added an explicit comment in Section 4.1.3 to clarify this.

**Manuscript change - L570-577:** *“On the contrary, for WET, no aggregation uncertainty is reported because this sector relies on a single wetland flux dataset for weighting, precluding a cross-inventory sensitivity assessment. We note, however, that the latitudinal contrast between tropical (more enriched,  $\sim -50\text{‰}$ ) and boreal (more depleted,  $\sim -70\text{‰}$ ) wetlands contributes substantially to the propagated uncertainty  $\sigma_{prop}$  already reported for this sector (0.4–8.2‰).”*

#### Table 5 – Tropical wetland measurements

**Reviewer comment:** “Maybe mention the France et al (2022) and Nisbet et al. (2022) tropical wetland results?? These were from both S. America and Africa...”

**Response:** We have added a sentence to Section 4.1.4 explicitly reporting the recent tropical airborne measurement values and comparing them with the values used in our maps.

**Manuscript change - L632-637:** *“Recent tropical airborne measurement programs report wetland source signatures of  $-59.0 \pm 1.3\text{‰}$  in Bolivian Amazonia (France et al., 2022) and  $-59.3 \pm 2.0\text{‰}$  for a Zambia–Bolivia composite (Nisbet et al., 2021), consistent with the tropical wetland values used in our maps from Oh et al. (2022). The slightly more enriched values produced by our maps over African papyrus-dominated wetlands likely reflect that these recent airborne measurements have not yet been assimilated into process-based wetland isotope models, contributing to the systematic biases on tropical wetlands discussed below.”*

#### L560 – China and India coal emissions

**Reviewer comment:** “China is dominant – but India is also a big coal emitter.”

**Response:** We have updated this sentence to explicitly mention India alongside China as a major coal-emitting region with relatively enriched signatures.

**Manuscript change: - L608** *“Our estimate is derived using flux-weighted averaging that emphasizes high-emitting coal regions, such as China and India, where emissions tend to be less depleted than the global average...”*

#### Table 6 – Stratospheric sink

**Reviewer comment:** “Chemistry – mention the stratospheric sink?”

**Response:** We have added a footnote to Table 6 explicitly noting that the Cl sink (which contributes both tropospheric and stratospheric components) is not perturbed independently in our sensitivity ensemble, with reference to the comprehensive analysis by Thanwerdas et al. (2022b) using the same model framework.

**Manuscript change:** *Footnote added to Table 6: “The Cl sink is not perturbed independently in this sensitivity ensemble. Its impact within the same ClF–LMDz–SACS framework has been*

*comprehensively quantified by Thanwerdas et al. (2022b), who report that stratospheric Cl alone contributes a ~0.30‰ surface enrichment in  $\delta^{13}\text{C}\text{-CH}_4$  via stratosphere–troposphere exchange, and modifies the seasonal cycle amplitude by 10–20% depending on latitude (see Sect. 4.2.3)."*

### L633 – Ethiopian cattle diet

**Reviewer comment:** "See Brychkova et al – Ethiopian cattle eat C<sub>3</sub> above about 2500m but around 2000m many forage grasses are C<sub>4</sub>."

**Response:** We thank the reviewer for this useful reference. We have incorporated Brychkova et al. (2022) into Section 4.2.1, in the discussion of regional AGW variability in Ethiopia, and again in Section 4.3.1 in the Indo-Gangetic Plain case study where we use Ethiopia as a finer-scale illustration.

**Manuscript change - L718-719:** *"For instance, in Ethiopia, the balance between C<sub>3</sub> and C<sub>4</sub> forage grasses varies with altitude, leading to distinct isotopic signatures within the same country (Brychkova et al., 2022)."*

**Manuscript change - L949-951:** *"The Ethiopian highlands provide a finer-scale illustration of this need: the C<sub>3</sub>/C<sub>4</sub> forage balance varies with altitude, producing sub-national contrasts in livestock signatures (Brychkova et al., 2022) that current global inventories cannot resolve. "*

### L671 – Landfills

**Reviewer comment:** "Maybe Nisbet et al 2020."

**Response:** We have added Nisbet et al. (2020) to the reference list in the discussion of waste management practices in Section 4.2.2 (L776).

### L687 – Caspian Sea classification

**Reviewer comment:** "This isn't clear – is the Caspian here treated as a Freshwater source? I think it's about 12‰ salinity... Also it has methane/mud volcanoes and there are huge petrochemical methane sources nearby – gasfields and oilfields."

**Response:** The reviewer raises a fair point. The Caspian Sea is indeed a brackish endorheic lake, and our classification of its emissions as freshwater is a default consequence of using the Stavert et al. (2022) lake-and-reservoir dataset, which does not separate brackish endorheic systems. We have clarified this explicitly in both Section 4.2.2 and Section 4.3.1, acknowledging the classification ambiguity, the brackish nature of the lake, and the proximity of major oil-and-gas infrastructure (Turkmenistan, Azerbaijan), which complicates regional source attribution.

**Manuscript change - L794-796:** *"The Caspian Sea is a large endorheic saline lake whose emissions are treated as freshwater in our framework given the absence of a dedicated dataset; its brackish nature and proximity to major oil and gas infrastructure introduce additional uncertainty in this region." (Section 4.2.2). And in Section 4.3.1 - L960-963: "The Caspian Sea is a large endorheic brackish lake, treated here as a freshwater source given the absence of a dedicated dataset for endorheic systems; this classification ambiguity, combined with proximity to major oil and gas infrastructure in Turkmenistan and Azerbaijan, makes regional source attribution particularly challenging."*

### L703 – Atmospheric chemistry concerns (Cl sink and stratospheric sink)

**Reviewer comment:** “I am concerned by two problems – 1) the Cl sink with its large isotopic leverage and 2) the stratospheric sink. Both of these seem poorly understood and with high uncertainty. Also note that OH in the tropical troposphere is changing (Morgenstern et al 2025) and likely has significant longitudinal variation around the globe.”

**Response:** Addressed in the responses to general comments G4 and G5 above. We have substantially expanded the chemistry discussion in Section 4.2.3, including a new paragraph on the Cl sink and its KIE leverage with reference to Allan et al. (2007), Wang et al. (2021), Saunio et al. (2025), Thanwerdas et al. (2022b) (L858-L873), and a discussion of the temporal and longitudinal variability of tropospheric OH following Morgenstern et al. (2025), Zhao et al. (2019) and Penn et al. (2025) (L823-829).

**Manuscript change - L823-829:** *“These regions also display marked longitudinal contrasts in tropospheric OH, driven by zonal asymmetries in convection, lightning NO<sub>x</sub>, and biomass burning, which are not consistently captured across global chemistry models (Zhao et al., 2019; Morgenstern et al., 2025).”*

### L715 – Oxidative capacity

**Reviewer comment:** “Could mention Ciais et al. 2026 and Nisbet & Manning 2026.”

**Response:** We have added both references to the discussion of OH-related uncertainties in Section 4.2.3.

**Manuscript change - L832:** *“This confirms that the oxidative sink is a dominant factor controlling methane concentrations and that its uncertainties propagate broadly rather than being confined to specific regions (Zhao et al., 2019; Ciais et al., 2026; Belikov et al., 2026; Nisbet and Manning, 2026; Skeie et al., 2023).”*

### L721 – Update older references

**Reviewer comment:** “References here are a bit elderly. ? Penn et al 2025, Skeie et al 2023?”

**Response:** We thank the reviewer for suggesting these references. We have added Skeie et al. (2023) alongside the existing citations on OH-driven CH<sub>4</sub> trends, as it directly examines how anthropogenic influence on OH through NO<sub>x</sub> and CO has modified the CH<sub>4</sub> growth rate over recent decades (L833). We have also added Penn et al. (2025) in the context of OH uncertainty characterization, as this study explores satellite-based constraints on tropospheric OH concentrations using GOSAT and AIRS observations, representing a promising avenue to reduce the OH-related uncertainties discussed in this section.

**Manuscript change - L829:** *“Satellite-based observations have also been explored as a means to better characterize tropospheric OH distributions and reduce these uncertainties (Penn et al., 2025).”*

## L918 – Targeted campaigns

**Reviewer comment:** “See MOYA – double volume of Phil Trans Royal Soc. 2021-2022.”

**Response:** We have explicitly cited the MOYA and ZWAMPS campaigns in Section 4.4 (Pathways for improvement) as examples of the type of coordinated airborne and ground-based campaigns needed to fill observational gaps in tropical regions.

**Manuscript change - L1042-1044:** *“Coordinated airborne and ground-based campaigns, exemplified by MOYA and ZWAMPS in tropical wetlands, rice fields, and biomass burning regions (Nisbet et al., 2021; France et al., 2022), provide a model for the type of effort needed to fill these observational gaps.”*

## Closing remarks

We thank Reviewer 1 once again for the very thorough and constructive review, and especially for the extensive list of references provided, which has substantially enriched the manuscript. We believe that the revisions, in particular the expanded treatment of latitudinal C<sub>3</sub>/C<sub>4</sub> gradients, the explicit acknowledgement of large freshwater and geological flux uncertainties, the strengthened discussion of the chlorine and stratospheric sinks, and the integration of recent tropical measurement programs, address all the concerns raised. We hope the revised manuscript will meet the expectations of the reviewer and the editor.

## Summary of new references added

In response to this review, the following references have been added to the manuscript:

- Allan, W., et al. (2007). Methane carbon isotope effects caused by atomic chlorine in the marine boundary layer. *J. Geophys. Res.: Atmospheres*, 112(D4).
- Barker, P. A. et al. (2020). Airborne measurements of fire emission factors for African biomass burning sampled during the MOYA campaign. *Atmos. Chem. Phys.*, 20, 15443–15459.
- Brychkova, G., et al. (2022). Climate change and land-use change impacts on future availability of forage grass species for Ethiopian dairy systems. *Sci. Rep.*, 12, 20512.
- Ciais, P., et al. (2026). Why methane surged in the atmosphere during the early 2020s. *Science*, 391, eadx8262.
- France, J. L., et al. (2022).  $\delta^{13}\text{C}$  methane source signatures from tropical wetland and rice field emissions. *Phil. Trans. R. Soc. A*, 380, 2215.
- Fujita, R., et al. (2025b). Global fossil methane emissions constrained by multi-isotopic atmospheric methane histories. *J. Geophys. Res.: Atmos.*, 130, e2024JD041266.
- Lan, X., et al. (2026). Trends in globally averaged CH<sub>4</sub> (Updated NOAA GML data, end-2025).
- Morgenstern, O., et al. (2025). Radiocarbon monoxide indicates increasing atmospheric oxidizing capacity. *Nature Communications*, 16, 249.

- Nisbet, E. G., & Manning, M. R. (2026). What is causing the methane surge? *Science*, 391, 556–557.
- Nisbet, E. G., et al. (2021/2022). Isotopic signatures of methane emissions from tropical fires, agriculture and wetlands: the MOYA and ZWAMPS flights. *Phil. Trans. R. Soc. A*, 380, 2215.
- Nisbet, E. G., et al. (2020). Methane mitigation: methods to reduce emissions, on the path to the Paris Agreement. *Reviews of Geophysics*, 58, e2019RG000675.
- Nisbet, E. G., et al. (2023). Atmospheric methane: comparison between methane's record in 2006–2022 and during glacial terminations.
- Penn, E., et al. (2025). What can we learn about tropospheric OH from satellite observations of methane? *Atmos. Chem. Phys.*, 25, 2947–2965.
- Petrenko, V. V., et al. (2017). Minimal geological methane emissions during the Younger Dryas–Preboreal abrupt warming event. *Nature*, 548, 443–446.
- Riddell-Young, B., et al. (2025). Microbial driver of 2006–2023 CH<sub>4</sub> growth indicated by trends in atmospheric δD–CH<sub>4</sub> and δ<sup>13</sup>C–CH<sub>4</sub>. *PNAS*, 122, e2516543122.
- Shaw, J. T., et al. (2022). Large methane emission fluxes observed from tropical wetlands in Zambia. *Global Biogeochem. Cycles*, 36, e2021GB007261.
- Skeie, R. B., et al. (2023). Trends in atmospheric methane concentrations since 1990 were driven and modified by anthropogenic emissions. *Comms. Earth & Envir.*, 4, 317.

## Response to Reviewer 2

## General response

We thank Reviewer 2 for the careful reading of the manuscript and for the constructive criticism. We are grateful that the reviewer recognises the timeliness and relevance of our work, the systematic uncertainty quantification, and the potential of the dataset to improve prior constraints in isotopic inversion systems. We have addressed all ten major comments through substantive revisions, including a new model–observation comparison section in the Supplement, an expanded critical assessment of inter-dataset systematic biases, additional sensitivity analyses on AGW sectoral granularity, an extended discussion of the OH-KIE parameterization and additional sinks (Cl, soil uptake), a new schematic diagram summarising the uncertainty propagation pathway, and a substantially revised discussion structure with improved readability and explicit regional case studies. We believe these revisions significantly strengthen the manuscript and address the concerns raised.

## Response to major comments

### M1. Absence of model–observation comparison

**Reviewer comment:** “The manuscript focuses on forward simulations and sensitivity analyses without comparison to atmospheric  $\delta^{13}\text{C}\text{-CH}_4$  observations. While the authors justify this choice, the absence of validation limits confidence in the dataset and its applicability. Please include at least a first-order comparison with available surface or global  $\delta^{13}\text{C}\text{-CH}_4$  observations to demonstrate the realism of the modeled fields.”

**Response:** We agree that some form of observational reference would strengthen confidence in the dataset, even though we maintain our methodological position that the central deliverables of this paper are (i) a transparent and reproducible  $\delta^{13}\text{C}\text{-CH}_4$  source signature dataset with quantified uncertainties, and (ii) a sensitivity analysis identifying the dominant uncertainty drivers. Full inversion-based validation, in which fluxes and signatures are jointly optimised, will be the subject of a follow-up study because forward simulations alone cannot disentangle biases on fluxes from biases on signatures.

To address the reviewer’s concern, we have added a new dedicated Section S4 “Model–observation comparison” in the Supplement, including two complementary first-order diagnostics:

(i) Globally averaged surface time series (1998–2022) of  $\text{CH}_4$  mole fraction and  $\delta^{13}\text{C}\text{-CH}_4$  for all forward sensitivity simulations, compared against the NOAA-INSTAAR globally averaged observations (Michel et al., 2024; Schuldt et al., 2025) with their  $\pm 1\sigma$  envelope (new Figure S11). This shows that most simulations remain within the observational envelope over the full period, while clearly identifying outliers (e.g., KIE\_CANTRELL and ANTHROPO\_GFEI) that are consistent with our sensitivity analysis findings.

(ii) Inter-hemispheric (NH–SH) gradient diagnostics for both  $\text{CH}_4$  and  $\delta^{13}\text{C}\text{-CH}_4$  averaged over 2016–2019 (new Figure S12). The inter-hemispheric gradient is a particularly stringent diagnostic because it isolates the joint contribution of source spatial distribution, transport, and oxidation

chemistry while being insensitive to absolute calibration offsets and spin-up drift. The reference configuration reproduces the observed  $\text{CH}_4$  gradient ( $\sim 0.117$  ppb) to within  $\sim 5\%$ . For  $\delta^{13}\text{C}-\text{CH}_4$ , all simulations underestimate the observed gradient ( $-0.32\text{‰}$  vs.  $-0.15$  to  $-0.25\text{‰}$  simulated), a residual bias which is fully consistent with our sensitivity analysis identifying OH-KIE and AGW source signatures as dominant drivers, and which reinforces our recommendations for inversion design.

We have also added a brief reference to this new comparison in the main text (Section 3.1.3) and in the Conclusions, while explicitly framing this as a plausibility reference rather than a formal validation, since forward simulations cannot rigorously validate the dataset without joint optimisation of fluxes and signatures.

**Manuscript change (Section 3.1.3, L 298–299):** “See Sect. S4 in the Supplementary Material for the full 1998–2022 time series of all simulations compared to NOAA-INSTAAR observations (Michel et al., 2024; Schuldt et al., 2025).”

**Manuscript change (Conclusions, L 1082–1085):** “This study focused on developing and evaluating updated  $\delta^{13}\text{C}-\text{CH}_4$  source signature maps through comparison with the literature, uncertainty quantification, and forward simulations. While direct validation using atmospheric data is beyond the scope of this paper, all necessary elements are provided, including gridded maps, uncertainty ranges, and sectoral breakdowns, to enable their integration into forward modeling and atmospheric inversions under optimal conditions.”

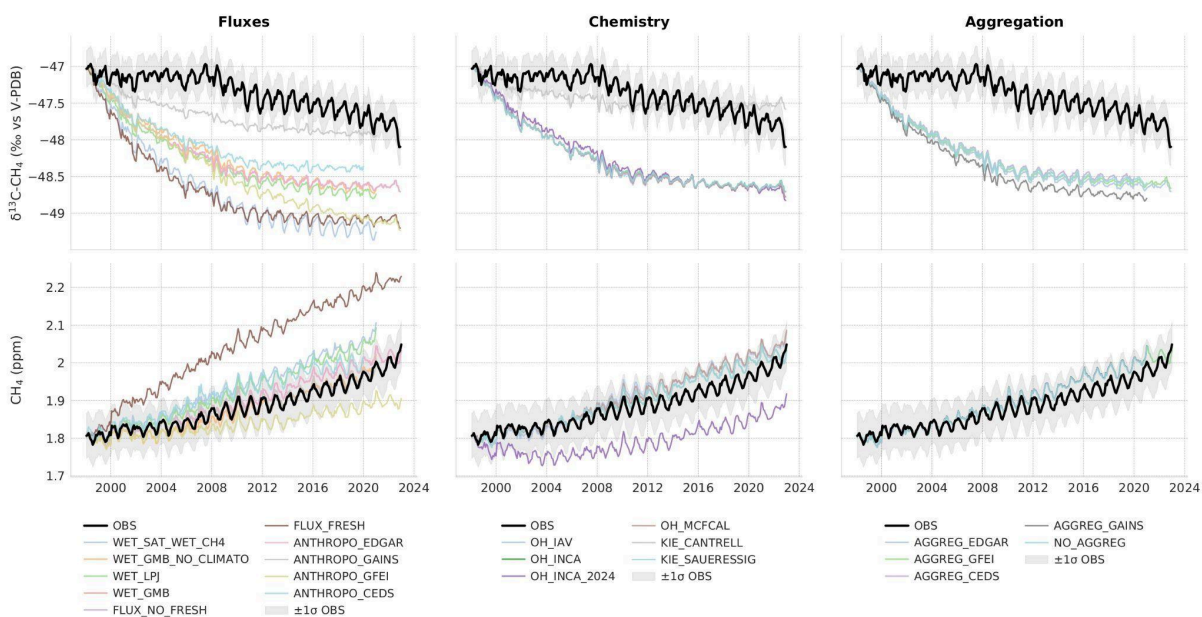


**Figure S11.** Globally averaged surface time series (1998–2022) of  $\delta^{13}\text{C}-\text{CH}_4$  signal (top row,  $\text{‰}$  vs V-PDB) and  $\text{CH}_4$  mole fraction (bottom row, ppm) for all forward sensitivity simulations described in Table 3 of the main text, grouped by perturbation category: Fluxes (left), Chemistry (middle) and Aggregation (right). Black solid line: NOAA-INSTAAR globally averaged observations (Michel et al., 2024; Schuldt et al., 2025); grey shading:  $\pm 1\sigma$  observational uncertainty. Coloured lines correspond to the individual simulations (see legends for configuration details). Simulations based on GAINS and GFEI inventories end in 2020 due to data availability.

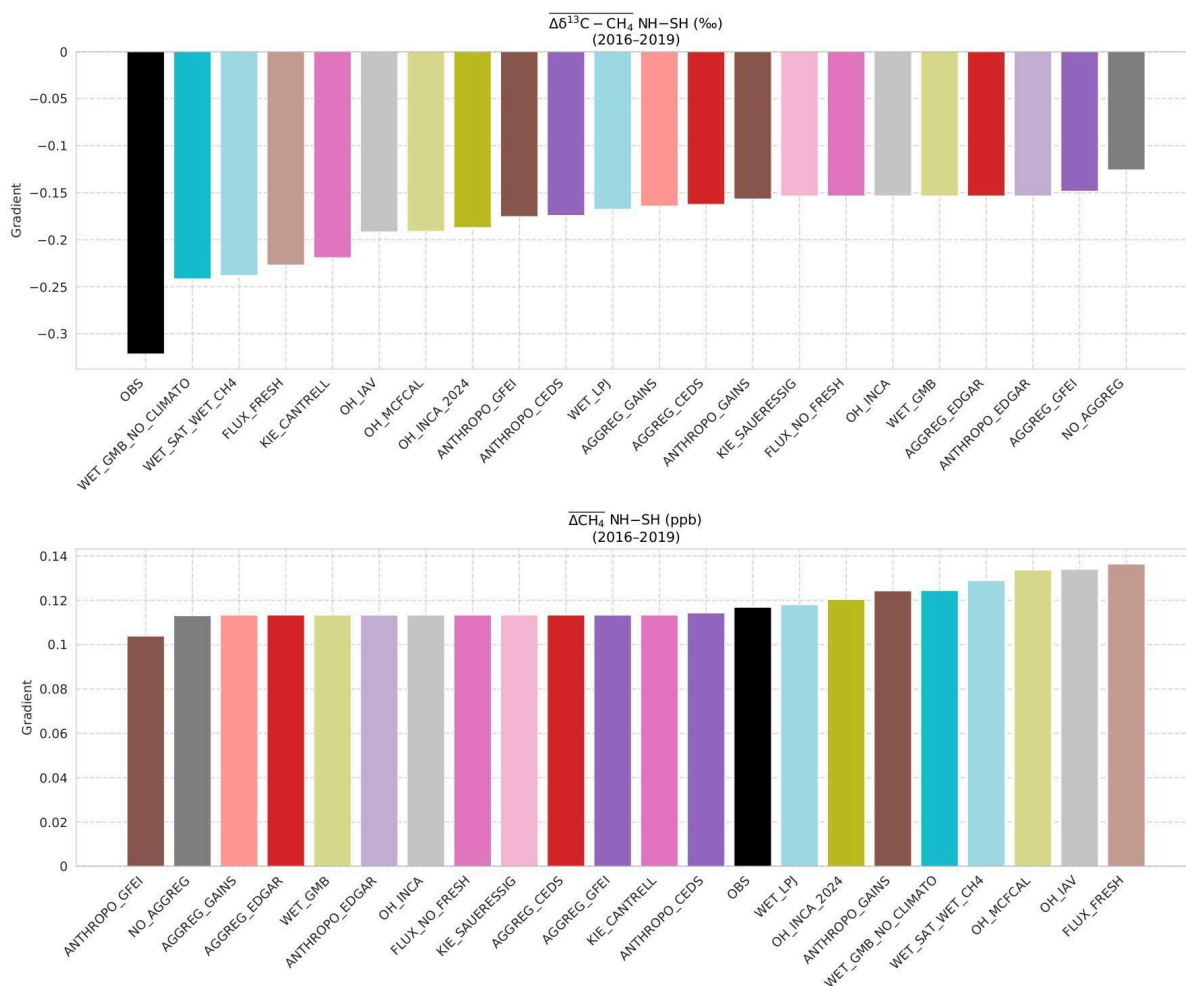


Figure S12. Inter-hemispheric gradient (NH-SH) of  $\delta^{13}\text{C}-\text{CH}_4$  (top, ‰ vs V-PDB) and  $\text{CH}_4$  (bottom, ppb) averaged over 2016–2019, for all forward sensitivity simulations described in Table 3 of the main text and for NOAA-INSTAAR observations (Michel et al., 2024; Schuldte et al., 2025) (black bar). Simulations are sorted by increasing gradient. The NH-SH gradient is computed from monthly surface fields, taking the difference between the latitudinally averaged Northern Hemisphere ( $0^\circ$ – $90^\circ\text{N}$ ) and Southern Hemisphere ( $90^\circ\text{S}$ – $0^\circ$ ) signals at the locations of NOAA-INSTAAR surface stations, and then averaged over 2016–2019.

## M2. Inter-dataset inconsistencies and systematic bias propagation

**Reviewer comment:** “The isotopic source maps are largely derived from previously published datasets and literature synthesis. While this approach is necessary, the manuscript does not sufficiently address the potential propagation of systematic biases. Provide a more critical assessment of inter-dataset inconsistencies and discuss how these uncertainties may influence the final isotopic maps.”

**Response:** We agree this point deserves a more critical treatment. We have substantially expanded Section 4.1.4 (Comparison with previous datasets) to include a new explicit discussion of three categories of systematic biases inherited from the underlying observational databases that are not captured by our quantitative  $\sigma_i$ :

(1) Uneven geographic coverage: the Sherwood et al. (2017, 2021) compilation underlying Lan et al. (2021a) is dominated by North American data; EMID (Menoud et al., 2024) improves European coverage but Africa, South America, and large parts of Asia remain under-sampled. Tropical wetlands are represented through fewer campaigns than boreal/temperate ones, and recent tropical measurement programs (France et al., 2022; Nisbet et al., 2021; Shaw et al., 2022) have not yet been integrated into process-based wetland isotope models.

(2) Methodological heterogeneity: literature signatures are typically arithmetic means while our sector values are flux-weighted; we explicitly quantify how this difference propagates for individual sub-sectors (e.g., the ~7‰ difference for coal between our flux-weighted estimate and the Menoud et al. (2022) arithmetic mean is shown to result from emphasis on high-emitting regions like China and India). For agricultural waste specifically, the inter-dataset spread (−52 to −57.8‰) exceeds the sub-sector uncertainty  $\sigma_i$ , pointing to genuine methodological heterogeneity in the definition of this sub-sector.

(3) Limited temporal representativeness: signatures are held constant for most sub-sectors over 1998–2022, while documented trends linked to evolving livestock feed composition, atmospheric  $\delta^{13}\text{C}$ – $\text{CO}_2$  changes, or gas processing practices (Chang et al., 2019) are not explicitly represented.

We have also added an explicit discussion of how these biases propagate to the aggregated maps depending on the flux-weighting scheme: biases affecting small-flux sub-sectors (termites, oceans) have limited impact, while those affecting high-emitting sub-sectors (livestock, oil and gas, tropical wetlands) propagate more directly to the modeled atmospheric  $\delta^{13}\text{C}$ – $\text{CH}_4$  signal, consistent with the sensitivity hierarchy reported in Table 6.

**Manuscript change (Section 4.1.4, L 644–661): “**

*Beyond these sub-sector-specific differences, the inter-dataset inconsistencies are of the same order as the sub-sector uncertainty  $\sigma_i$  and point to systematic biases inherited from the underlying observational databases, which  $\sigma_i$  does not capture. At the sub-sector level,  $\sigma_i$  reflects the statistical dispersion within the sampled measurements (Menoud et al., 2022), not the representativeness of that sample relative to the true global distribution of emission sources. We identify three main systematic biases:*

*– Uneven geographic coverage: the compilation from Sherwood et al. (2017, 2021) underlying Lan et al. (2021a) is dominated by North American data, EMID (Menoud et al., 2024) improves European coverage but Africa, South America, and large parts of Asia remain under-sampled; tropical wetlands are represented through fewer campaigns than boreal/temperate ones, and recent tropical measurement programs (France et al., 2022; Nisbet et al., 2021; Shaw et al., 2022) have not yet been integrated;*

*– Methodological heterogeneity: literature signatures are arithmetic means while our sector values are flux-weighted;*

– Limited temporal representativeness: signatures are held constant for most sub-sectors over 1998–2022, while documented trends linked to evolving livestock feed composition or gas processing practices (Chang et al., 2019) are not explicitly represented.

*The propagation of these biases to the aggregated maps depends on the flux-weighting scheme: biases affecting small-flux sub-sectors (termites, oceans) have limited impact, while those affecting high-emitting sub-sectors (livestock, oil & gas, tropical wetlands) propagate more directly to the modeled atmospheric  $\delta^{13}\text{C}-\text{CH}_4$  signal, consistent with the sensitivity hierarchy reported in Table 6.*

### M3. Finer disaggregation of the AGW sector

**Reviewer comment:** “The agriculture and waste sector is identified as the dominant source of uncertainty, yet it is treated in a relatively aggregated manner. Where possible, further disaggregate AGW into sub-categories (e.g., livestock, rice paddies, waste management), or include sensitivity analyses demonstrating the effect of finer sectoral partitioning.”

**Response:** We agree that AGW deserves particular attention given its dominant role. We would like to clarify that AGW is in fact already disaggregated in our framework into five sub-sectors (livestock, rice, landfills, wastewater, agricultural waste), each with its own isotopic signature and flux distribution (Table 1). Both the aggregated five-sector maps and the underlying 14 sub-sector maps are publicly distributed (Code and data availability section), so users can re-aggregate according to their own classification.

We have addressed the reviewer’s concern through three substantive additions:

(1) Explicit AGW sub-sector breakdown in Section 4.2.1: we now state that livestock and rice together account for ~62% of AGW emissions and carry the most depleted signatures ( $-65.8\text{‰}$  and  $-59.9\text{‰}$ ), while waste-related sub-sectors ( $-50.9$  to  $-56.2\text{‰}$ ) make up the remaining 38%. This contrast is the main driver of the propagated uncertainty  $\sigma_{\text{prop}}$  reported for AGW in Table 4.

(2) Explaining into more details the NO\_AGGREG sensitivity simulation: we investigate the dedicated test in which the number of source categories transported in the atmospheric model was increased from 5 to 14 (full sub-sector resolution), to evaluate the trade-off between computational efficiency and isotopic detail. The resulting differences in modeled atmospheric  $\delta^{13}\text{C}-\text{CH}_4$  are small at global scale ( $+0.06\text{‰}$  mean), with localized differences of up to  $\pm 0.5\text{‰}$  in regions where sub-sector composition contrasts strongly with the global average (notably South Asia and the Middle East; see new Figure S4). This indicates that the limiting factor for AGW-related uncertainty is not the number of categories but rather the signature values of the existing sub-sectors and inventory-level flux partitioning between livestock and waste.

(3) Indo-Gangetic Plain regional case study (Section 4.3.1): we now show that AGW source signatures contribute up to 80% of local  $\delta^{13}\text{C}-\text{CH}_4$  variance over this region, driven by the strong contrast between livestock and waste sub-sectors, with the relative livestock share varying from 67% (EDGARv8) to 79% (CEDS, GAINS) across inventories.

**Manuscript change (Section 4.2.1, L 719–733):** “AGW is disaggregated in our framework into five sub-sectors (livestock, rice, landfills, wastewater, and agricultural waste; Table 1), each with its own isotopic signature and flux distribution. Livestock and rice together account for ~62% of AGW emissions and carry the most depleted signatures ( $-65.8\text{‰}$  and  $-59.9\text{‰}$ ), while waste-related sub-sectors ( $-50.9$  to  $-56.2\text{‰}$ ) make up the remaining 38%. This contrast is the main driver of the propagated uncertainty  $\sigma_{\text{prop}}$  reported for AGW in Table 4. To assess whether finer sectoral granularity, i.e. the number of source categories effectively resolved in the atmospheric model, would meaningfully change the modeled atmospheric signal, the NO\_AGGREG simulation increases the number of source categories from 5 to 14 (Table 3). This is conceptually distinct from the aggregation uncertainty  $\sigma_{\text{agg}}$  defined in Sect. 2.3.3, which quantifies the sensitivity of the aggregated signature to the choice of flux inventory used for weighting. The resulting differences are small:  $+0.061\text{‰}$  globally for  $\delta^{13}\text{C-CH}_4$  (Fig. S4). Localized differences of up to  $\pm 0.5\text{‰}$  in  $\delta^{13}\text{C-CH}_4$  occur in regions where sub-sector composition contrasts strongly with the global average, notably in South Asia and the Middle East. These results indicate that increasing sectoral granularity beyond five sub-sectors does not substantially alter the modeled atmospheric isotopic signal at the global scale. Reducing AGW-related uncertainty would therefore benefit more from better-constraining the signature values of the existing sub-sectors and from refining inventory-level flux partitioning between livestock and waste, particularly in rapidly developing regions, than from increasing the number of source categories.”

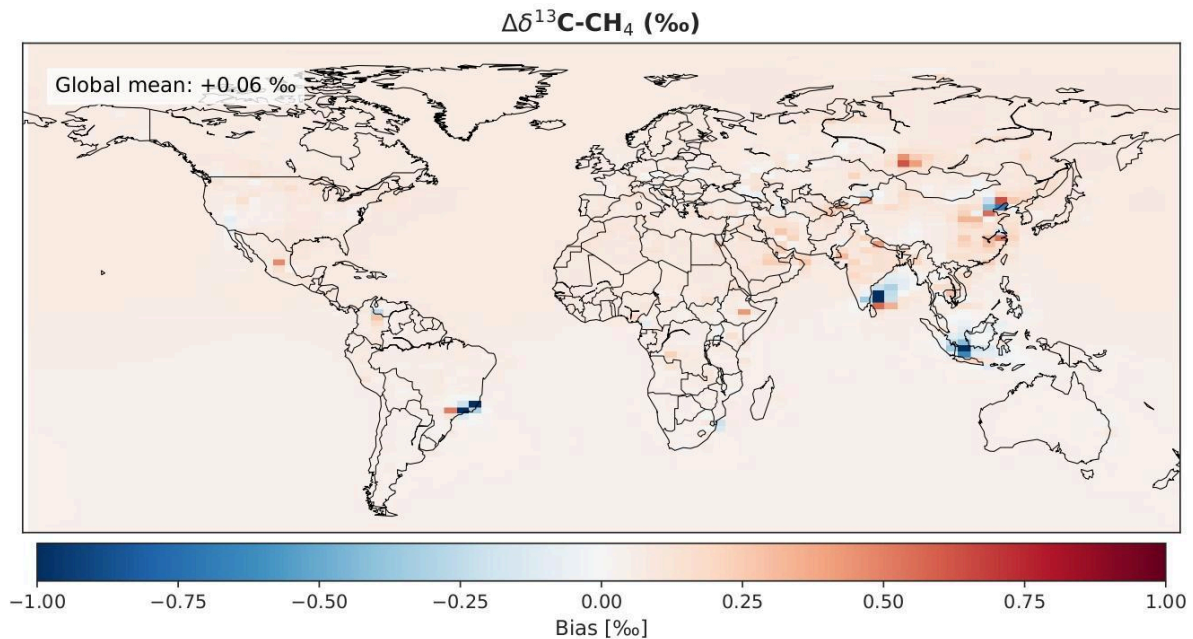


Figure S4. Difference maps between the NO\_AGGREG (14 categories) and the reference OH\_INCA simulation (5 categories) averaged over 2016–2020 at the surface level for  $\Delta\delta^{13}\text{C-CH}_4$  (‰).

#### M4. Treatment of the OH kinetic isotope effect

**Reviewer comment:** “The results highlight OH-KIE as a dominant driver of  $\delta^{13}\text{C-CH}_4$  uncertainty, yet the treatment of this process is relatively simplified. Please expand the discussion of OH-KIE

parameterization, including laboratory constraints, variability, and implications for inversion systems.”

**Response:** We agree this is an important point given the dominant role of OH-KIE. We have substantially expanded the discussion in Section 4.2.3 to cover:

(1) Laboratory constraints: the OH-KIE estimate relies on only two published experimental determinations (Cantrell et al. (1990):  $1.0054 \pm 0.0009$  at 296 K; Saueressig et al. (2001):  $1.0039 \pm 0.0004$  at 296 K). No measurements exist below 278 K, although theoretical calculations suggest the KIE may increase at lower temperatures (Gupta et al., 1997).

(2) Atmospheric leverage: at steady state, Fujita et al. (2020) showed that the 0.0015 difference between the two values yields a  $\sim 1.3\text{‰}$  shift in atmospheric  $\delta^{13}\text{C-CH}_4$ . This high leverage explains why our sensitivity analysis ranks OH-KIE as the dominant chemistry-related driver of  $\delta^{13}\text{C-CH}_4$  variability (RSD 2.2%, SD 0.40‰; Table 6).

(3) Practical implications for inversions: previous  $\delta^{13}\text{C-CH}_4$  inversions have adopted either value (Saueressig et al. (2001) in Nisbet et al. (2016); Schaefer et al. (2016); Basu et al. (2022); Thanwerdas et al. (2024); Cantrell et al. (1990) in Rice et al. (2016)). This choice is absorbed by the posterior source mixture and represents an intrinsic uncertainty that cannot be reduced through prior refinement.

(4) Recommendation: we now recommend treating the full Cantrell–Saueressig range in inversion frameworks (see Section 4.3.2), either through ensemble-based approaches or explicit optimization within variational frameworks, until laboratory or theoretical advances narrow this range.

**Manuscript change (Section 4.2.3, L 846–854):** *“Regarding the kinetic isotope effect, Figure 6f and Figure S5f show that uncertainties in the OH-KIE induce a geographically homogeneous SD of 0.4‰ (RSD of 2.2%) in the atmospheric  $\delta^{13}\text{C-CH}_4$  signal, exceeding the observed SD at surface stations. This sensitivity is driven by only two published experimental determinations of the  $^{12}\text{C}/^{13}\text{C}$  KIE for  $\text{CH}_4 + \text{OH}$ : Cantrell et al. (1990) ( $1.0054 \pm 0.0009$  at 296 K) and Saueressig et al. (2001) ( $1.0039 \pm 0.0004$  at 296 K). No measurements exist below 278 K, although theoretical calculations suggest the KIE may increase at lower temperatures (Gupta et al., 1997). At steady state, Fujita et al. (2020) showed that the 0.0015 difference between the two values yields a  $\sim 1.3\text{‰}$  shift in atmospheric  $\delta^{13}\text{C-CH}_4$ , illustrating the high leverage of this parameter. In practice, previous inversions have adopted either value, Saueressig et al. (2001) in e.g. Nisbet et al. (2016); Schaefer et al. (2016); Basu et al. (2022); Thanwerdas et al. (2024), and Cantrell et al. (1990) in e.g. Rice et al. (2016). This choice is absorbed by the posterior source mixture. Accordingly, we recommend treating the full Cantrell–Saueressig range in inversion frameworks (see Sect. 4.3.2)”*

## M5. Other sinks: Cl oxidation and soil uptake

**Reviewer comment:** “The manuscript primarily focuses on OH oxidation, while other sinks (e.g., Cl oxidation, soil uptake) receive limited attention. Provide a more quantitative discussion of these additional sinks and their potential isotopic impacts.”

**Response:** We agree this deserves a quantitative treatment. We have added a dedicated paragraph in Section 4.2.3 covering both sinks:

Chlorine sink: We now explicitly discuss its magnitude ( $\sim 1\text{--}3\%$  of total  $\text{CH}_4$  oxidation; Hossaini et al., 2016; Sherwen et al., 2016; Gromov et al., 2018; Wang et al., 2021), the climatological tropospheric Cl sink of 6 [1–13] Tg  $\text{CH}_4 \text{ yr}^{-1}$  reported by the latest Global Methane Budget (Saunio et al., 2025), and its exceptionally large KIE ( $\approx 1.066$  at 298 K; Saueressig et al., 1995) which is more than an order of magnitude larger than that of OH. We provide a quantitative reference to Thanwerdas et al. (2022b), who quantified within the same CIF–LMDz–SACS framework as ours that mean tropospheric Cl perturbations of 1000 molec.  $\text{cm}^{-3}$  induce a near-linear sensitivity of  $+11.7 \text{ Tg CH}_4 \text{ yr}^{-1}$  and  $-1.0\%$  in the globally averaged source signature, with stratospheric Cl alone contributing a  $\sim 0.30\%$  surface enrichment in  $\delta^{13}\text{C-CH}_4$  via stratosphere–troposphere exchange. We explain that we did not repeat a Cl sensitivity experiment because it would essentially duplicate this recent and comprehensive analysis with the same model, but we acknowledge the Cl sink as a leading factor limiting isotope-based source partitioning, in agreement with Basu et al. (2022) and Röckmann et al. (2024b).

Soil sink: We now explicitly discuss its magnitude ( $\sim 31$  [17–39] Tg  $\text{CH}_4 \text{ yr}^{-1}$ , Saunio et al., 2025, or about 5% of the total  $\text{CH}_4$  sink), its moderate KIE ( $\approx 1.020$ ; Snover and Quay, 2000), intermediate between OH (1.0039) and Cl (1.066), and its dynamic implementation in our framework (first-order deposition process with isotope-dependent deposition velocities; Section 3.1.5). We argue that, given its small relative contribution, its moderate KIE, and its well-constrained global magnitude, soil uptake uncertainties are expected to have a substantially smaller impact on the modeled  $\delta^{13}\text{C-CH}_4$  signal than OH-KIE, and were therefore not perturbed in the Monte Carlo ensemble.

We also added a footnote to Table 6 explicitly noting that the Cl sink is not perturbed independently in our sensitivity ensemble, with reference to Thanwerdas et al. (2022b).

**Manuscript change (Section 4.2.3, new paragraph L 855–879): “**

*Beyond OH, two additional sinks contribute to the  $\delta^{13}\text{C-CH}_4$  budget and deserve explicit discussion: oxidation by chlorine (Cl) and soil uptake. Both are included in our forward simulations (Sect. 3.2) but were not perturbed in dedicated sensitivity experiments.*

*The Cl sink accounts for a small fraction of total  $\text{CH}_4$  oxidation. Recent estimates converge on a tropospheric contribution of  $\sim 1\text{--}3\%$  of the total chemical sink (Hossaini et al., 2016; Sherwen et al., 2016; Gromov et al., 2018; Wang et al., 2021), with the latest Global Methane Budget reporting a climatological tropospheric Cl sink of 6 [1–13] Tg  $\text{CH}_4 \text{ yr}^{-1}$  (Saunio et al., 2025), substantially smaller and better constrained than earlier estimates (Allan et al., 2007). Despite this small magnitude, the Cl reaction carries an exceptionally large kinetic isotope effect (KIE  $\approx 1.066$  at 298 K; Saueressig et al., 1995), more than an order of magnitude larger than that of OH, so even modest uncertainties in Cl concentrations translate into substantial shifts in modeled  $\delta^{13}\text{C-CH}_4$  (see Table 2). Basu et al. (2022) further identified the combined uncertainty in fractionation (OH-KIE and Cl contribution) as the single most important factor limiting isotope-based source partitioning at the global scale (Röckmann et al., 2024b). Thanwerdas et al. (2022b) quantified this influence within the same CIF–LMDz–SACS framework used here, and reported a near-linear sensitivity of  $+11.7 \text{ Tg CH}_4 \text{ yr}^{-1}$  and  $-1.0\%$  in the*

globally averaged source signature per 1000 molec. cm<sup>-3</sup> increase in mean tropospheric Cl, with stratospheric Cl alone contributing a ~ 0.30 ‰ surface enrichment via stratosphere–troposphere exchange and modifying the δ<sup>13</sup>C-CH<sub>4</sub> seasonal cycle amplitude by up to 10–20% depending on latitude. Because our configuration adopts the Cl field from Wang et al. (2021), consistent with the most recent tropospheric chlorine chemistry, the Cl-related uncertainty in our simulations is bounded by the ranges quantified in Thanwerdas et al. (2022b), which are of the same order of magnitude as the OH-KIE sensitivity reported in Table 6. A dedicated Cl sensitivity experiment was therefore not repeated here to avoid duplicating a recent and comprehensive analysis with the same model.

Soil uptake contributes ~ 31 [17–39] Tg CH<sub>4</sub> yr<sup>-1</sup> to the global CH<sub>4</sub> budget (Saunio et al., 2025), or about 5% of the total CH<sub>4</sub> sink, with a moderate KIE of ~ 1.020 (Snover and Quay, 2000), intermediate between OH (1.0039) and Cl (1.066) (see Table 2). In our framework, it is implemented as a first-order deposition process with isotope-dependent deposition velocities (Sect. 3.1.5). Given its small relative contribution to the total sink, its moderate KIE, and the well-constrained global magnitude reported in recent budgets, soil uptake uncertainties are expected to have a substantially smaller impact on the modeled δ<sup>13</sup>C-CH<sub>4</sub> signal than the OH-KIE (Table 6), and were therefore not perturbed in the Monte Carlo ensemble.”

## M6. Schematic of the uncertainty propagation methodology

**Reviewer comment:** “The uncertainty propagation methodology is rigorous but complex and may be difficult for readers to follow. Maybe include a schematic diagram summarizing uncertainty components and clarify how these uncertainties are incorporated into inversion prior error structures.”

**Response:** We agree, this is a very useful suggestion. We have added a new Figure 1 to Section 2.3, which provides a schematic overview of the full uncertainty propagation pathway:

- Sub-sector isotopic uncertainties  $\sigma_i$ , derived from Monte Carlo simulations (lower bound) and literature standard deviations (upper bound);
- Propagation to the sector level ( $\sigma_{prop}$ ) via flux-weighted error propagation (Eq. 3);
- Aggregation uncertainty ( $\sigma_{agg}$ ), estimated from sensitivity tests using different emission inventories (Eq. 5);
- Combination into total sectoral uncertainty ( $\sigma_{total}$ , Eq. 2; Table 4);
- Use of  $\sigma_{total}$  in inversion frameworks: either to inform the prior error covariance matrix B (if isotopic source signatures are optimised), or the observation error covariance matrix R (if they are held fixed).

We also added an introductory paragraph in Section 2.3 referencing this new schematic and laying out the overall structure of the propagation chain. Combined with the Figure 4 (showing how uncertainties propagate through the inversion) and the Figure 10 (clarifying the effect of including δ<sup>13</sup>C-CH<sub>4</sub> constraints in the inversion), readers now have a complete visual narrative from sub-sector measurements to inversion error structures.

**Manuscript change (Section 2.3, new introductory paragraph L 190–194):** “This section describes how uncertainties in aggregated  $\delta^{13}\text{C}\text{-CH}_4$  source signatures are estimated. (...) The overall propagation pathway, from sub-sector measurements to inversion error structures, is summarized schematically in Fig. 1. In what follows, we describe the three components of this propagation chain: the total uncertainty  $\sigma_{\text{total}}$  combining all contributions (Sect. 2.3.1), the propagated uncertainty  $\sigma_{\text{prop}}$  derived from sub-sector variability (Sect. 2.3.2), and the aggregation uncertainty  $\sigma_{\text{agg}}$  reflecting inventory choices (Sect. 2.3.3).”

**New Figure 1:** Schematic overview of the uncertainty propagation pathway for  $\delta^{13}\text{C}\text{-CH}_4$  source signatures, linking sub-sector uncertainties ( $\sigma_i$ ) through flux-weighted propagation ( $\sigma_{\text{prop}}$ ) and inventory-based aggregation tests ( $\sigma_{\text{agg}}$ ) to the total sectoral uncertainty ( $\sigma_{\text{total}}$ ), and then to the B and R matrices in atmospheric inversion frameworks.

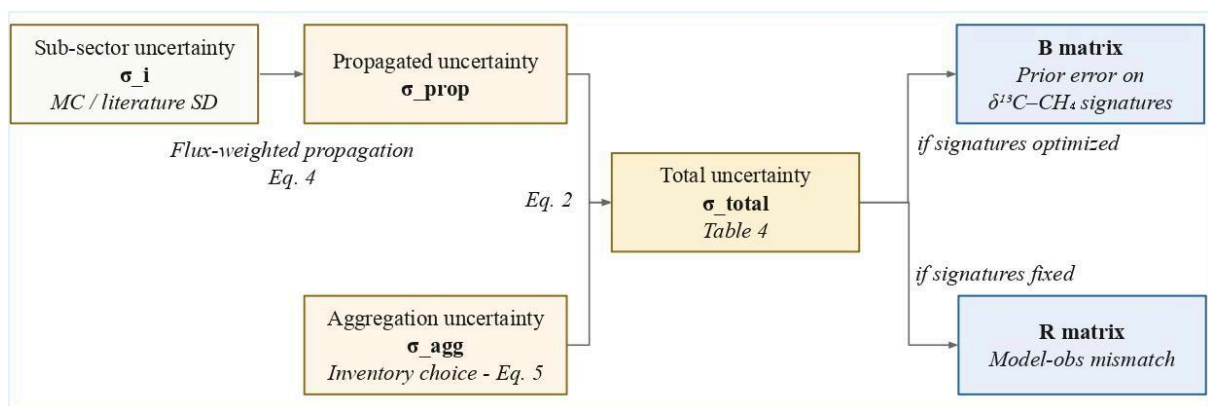


**Fig.1** Schematic overview of the uncertainty propagation pathway for  $\delta^{13}\text{C}\text{-CH}_4$  source signatures. Sub-sector isotopic uncertainties ( $\sigma_i$ ), derived from Monte Carlo simulations (lower bound) and literature standard deviations (upper bound), are propagated to the sector level ( $\sigma_{\text{prop}}$ ) via flux-weighted error propagation (Eq. 3). The aggregation uncertainty ( $\sigma_{\text{agg}}$ ), estimated from sensitivity tests using different emission inventories (Eq. 5), is combined with  $\sigma_{\text{prop}}$  to yield the total sectoral uncertainty ( $\sigma_{\text{total}}$ , Eq. 2). In atmospheric inversion frameworks,  $\sigma_{\text{total}}$  informs either the prior error covariance matrix (B) if isotopic source signatures are optimized, or the observation error covariance matrix (R) if they are held fixed (see Sect. 4.3.2)

## M7. Single transport model (LMDz)

**Reviewer comment:** “All simulations are conducted using a single atmospheric transport model (LMDz), without discussion of model-related uncertainties. Discuss the potential influence of transport model choice and resolution on the results.”

**Response:** We acknowledge this limitation, which is intrinsic to a single-model study. We have added a dedicated discussion in Section 4.4 (Pathways for improvement) addressing transport-related uncertainty in three respects:

(1) Model spread for CH<sub>4</sub> budgets: the TransCom-CH<sub>4</sub> intercomparison (Patra et al., 2011) showed that modeled CH<sub>4</sub> budgets are sensitive to troposphere–stratosphere exchange rates and to vertical grid structure, with CH<sub>4</sub> lifetimes spanning 9.50–10.27 yr across 12 CTMs using identical OH fields.

(2) Specific implications for  $\delta^{13}\text{C}\text{-CH}_4$ : vertical transport additionally controls the rate at which <sup>13</sup>C-enriched stratospheric air re-enters the troposphere via the Brewer–Dobson circulation, as well as the vertical distribution of the Cl sink and its strong fractionation (Butchart, 2014; Thanwerdas et al., 2022b).

(3) Robustness argument: the sensitivity hierarchy identified in our study (dominated by OH-KIE and AGW signatures) is driven by prescribed inputs (oxidant fields, source signatures) rather than by transport, and is therefore expected to be robust across CTMs. Quantifying transport-related uncertainty through multi-model ensembles, by extending the TransCom-CH<sub>4</sub> framework to include both CH<sub>4</sub> and  $\delta^{13}\text{C}\text{-CH}_4$ , remains a priority for future work and complements the dataset distributed here, which can be used by other inversion systems with their own transport models.

We also explicitly acknowledge the LMDz horizontal resolution (3.75° × 1.875°) in Section 3.1.1 and now state in Section 4.4 that “all simulations were performed with LMDz at a single resolution” as a caveat.

**Manuscript change (Section 4.4, transport paragraph L 1029–1038):** *“A second priority concerns atmospheric transport and chemistry, which were not perturbed in our sensitivity ensemble. All simulations were performed with LMDz at a single resolution (Sect. 3.1.1), and the TransCom-CH<sub>4</sub> intercomparison (Patra et al., 2011) showed that modeled CH<sub>4</sub> budgets are sensitive to troposphere–stratosphere exchange rates and to vertical grid structure, with CH<sub>4</sub> lifetimes spanning 9.50–10.27 yr across 12 CTMs using identical OH fields. For  $\delta^{13}\text{C}\text{-CH}_4$ , vertical transport additionally controls the rate at which <sup>13</sup>C-enriched stratospheric air re-enters the troposphere via the Brewer–Dobson circulation. The sensitivity hierarchy identified here, dominated by OH-KIE and AGW signatures, is driven by prescribed inputs and is expected to be robust across CTMs, but quantifying transport-related uncertainty through multi-model ensembles remains a priority.”*

## M8. Detailed regional analyses

**Reviewer comment:** “The manuscript identifies regions with high isotopic uncertainty but does not explore them in depth. Include more detailed regional analyses or case studies, particularly for key methane-emitting regions.”

**Response:** We agree this is essential, especially because Figure 9 (now extensively discussed) reveals that the dominant uncertainty drivers are strongly heterogeneous across the globe. We have added three explicit regional case studies in Section 4.3.1:

(1) Indo-Gangetic Plain: AGW source signatures contribute up to 80% of the local  $\delta^{13}\text{C}\text{-CH}_4$  variance over this region. We quantify both the magnitude (~26 Tg CH<sub>4</sub> yr<sup>-1</sup> from EDGARv8 over 2016–2020) and the source of the spread (relative livestock share varies from 67% in EDGARv8 to 79% in CEDS/GAINS, generating direct propagation to atmospheric  $\delta^{13}\text{C}\text{-CH}_4$ ). The Ethiopian highlands

provide a finer-scale illustration of the C<sub>3</sub>/C<sub>4</sub> forage balance varying with altitude (Brychkova et al., 2022). We also reference emerging dual-isotope evidence over South Asia (Yao et al., 2026).

(2) Tropical wetlands (Congo Basin, Amazon, Borneo): wetland flux uncertainties dominate, reaching more than 60% of local variance in Borneo. We note that recent tropical airborne and ground-based campaigns (France et al., 2022; Nisbet et al., 2021; Shaw et al., 2022) have begun addressing the data gap but cover only a limited number of sites.

(3) Caspian region: freshwater flux uncertainties account for more than 60% of local  $\delta^{13}\text{C}\text{-CH}_4$  variance, due to the classification ambiguity of this brackish endorheic lake combined with proximity to major oil and gas infrastructure in Turkmenistan and Azerbaijan.

These regional analyses are then linked to a key conceptual distinction in Section 4.3.2 between two regimes of uncertainty: localized hotspots, where targeted external efforts (inventories, field campaigns, process models) can reduce prior errors, and remote/well-mixed background regions, where uncertainties are dominated by OH-KIE and require explicit optimization within the inversion framework.

**Manuscript change (Section 4.3.1, new regional case studies subsection L 942–965):** *“Four regional case studies illustrate the diversity of dominant drivers and provide context for the targeted improvements discussed in Sect. 4.3.2 and Sect. 4.4. – Indo-Gangetic Plain: AGW source signatures contribute up to 80% of the local  $\delta^{13}\text{C}\text{-CH}_4$  variance (...). – Tropical wetlands (Congo Basin, Amazon, Borneo): Wetland flux uncertainties dominate over these regions, reaching more than 60% of local  $\delta^{13}\text{C}\text{-CH}_4$  variance in Borneo (...). – Caspian region: Freshwater flux uncertainties account for more than 60% of the local  $\delta^{13}\text{C}\text{-CH}_4$  variance (...).”*

## M9. Satellite observations – quantitative limitations

**Reviewer comment:** “The manuscript includes a forward-looking discussion on satellite observations (e.g., GOSAT, TROPOMI), but this remains largely conceptual. Clarify current technical limitations and, if possible, provide quantitative estimates of detection capabilities.”

**Response:** We agree, the satellite discussion was too conceptual. We have substantially revised the corresponding paragraph in the Conclusions to provide quantitative estimates of detection capabilities, and we now address two distinct issues:

(1) Precision gap: Malina et al. (2019) report individual  $^{13}\text{CH}_4$  retrieval uncertainties of <1 ppb for TROPOMI and <0.68 ppb (<0.2 ppb in high-SNR cases) for Sentinel-5/UVNS, whereas the target  $\delta^{13}\text{C}$  uncertainty of <1‰ required to differentiate source types corresponds to a  $^{13}\text{CH}_4$  uncertainty of <0.02 ppb, a gap of one to two orders of magnitude that requires significant spatial and/or temporal averaging.

(2) Systematic errors:  $^{13}\text{CH}_4$  retrievals are highly sensitive to errors in a priori temperature and pressure profiles (Malina et al., 2019).

A dedicated detectability assessment is planned as a follow-up to the present work, building on the isotopic maps and sensitivity framework developed here, and aiming to quantify the spatial and temporal scales at which GOSAT, TROPOMI and IASI could detect  $\delta^{13}\text{C}\text{-CH}_4$  signals above their respective noise floors. We mention it to indicate the trajectory of follow-up work that the present dataset is designed to support.

**Manuscript change (Conclusions, satellite paragraph L 1086–1095):** *“Finally, the increasing availability of satellite-based  $\text{CH}_4$  and isotopic measurements opens promising perspectives for constraining methane sources at the global scale. (...) Individual  $^{13}\text{CH}_4$  retrieval uncertainties remain large: Malina et al. (2019) report mean uncertainties of  $<1$  ppb for TROPOMI (SWIR3 channel) and  $<0.68$  ppb for Sentinel-5/UVNS (SWIR1 channel), whereas the target  $\delta^{13}\text{C}$  uncertainty of  $<1\text{‰}$  required to differentiate between source types corresponds to a  $^{13}\text{CH}_4$  uncertainty of  $<0.02$  ppb. Significant spatial and/or temporal averaging is therefore required to reduce uncertainties to detectable levels. In addition,  $^{13}\text{CH}_4$  retrievals are highly sensitive to errors in a priori temperature and pressure profiles, which can introduce systematic biases (Malina et al., 2019). A dedicated detectability assessment will be essential to evaluate whether current or forthcoming missions can effectively detect and interpret atmospheric isotopic variations under real conditions.”*

#### M10. Readability of uncertainty propagation and sensitivity analysis sections

**Reviewer comment:** “While the manuscript is generally well organized, some sections, particularly those describing uncertainty propagation and sensitivity analyses, are dense and difficult to follow. Please improve readability by summarizing key findings at the end of sections and reducing redundancy between the Results and Discussion.”

**Response:** We agree, this is a fair criticism, and we have implemented several structural improvements:

(1) End-of-section summaries: we added concise summary paragraphs at the end of each main results sub-section (4.1.1, 4.1.2, 4.1.3, 4.2.1, 4.2.2, 4.2.3, 4.2.4) highlighting the key findings in 2–3 sentences. For example, Section 4.2.1 now ends with: “In summary, two distinct aggregation-related effects have been tested in this section. (...) Both aggregation-related choices therefore have a limited impact on atmospheric simulations, supporting the transferability of the updated maps across inversion systems and inventories.”

(2) Restructured Discussion: Section 4.3 has been reorganised into three clearly-distinguished sub-sections: 4.3.1 Key uncertainty drivers (synthesis of sensitivity results, no redundancy with Section 4.2); 4.3.2 Implications for isotopic inversions (recommendations only, with practical bullet points); 4.3.3 Pathways for improvement (renumbered and restructured into three thematic axes: temporal representativeness, transport and chemistry, process-level understanding).

(3) Reduced redundancy: we systematically removed text overlapping between Sections 4.2 and 4.3. Section 4.3.1 now references Section 4.2 results without re-explaining them, focusing instead on integration and ranking.

We hope these revisions substantially improve readability while preserving the rigour of the methodology.

## Closing remarks

We thank Reviewer 2 once again for the constructive critique. We believe the revisions outlined above, including the new model–observation comparison (Section S4 of the Supplement), the explicit treatment of inter-dataset systematic biases, the additional NO\_AGGREG sensitivity simulation, the expanded chemistry discussion (OH-KIE, Cl, soil uptake), the new schematic figure (Fig. 1), the regional case studies, the quantitative satellite assessment, and the structural improvements in readability, address all ten major comments. We are confident the revised manuscript is substantially strengthened and we hope it now meets the expectations of the reviewer and the editor.

## Summary of new material added in response to Reviewer 2

- New Figure 1 (Section 2.3): schematic overview of the uncertainty propagation pathway from sub-sectors to inversion B/R matrices.
- Substantial revision to NO\_AGGREG sensitivity simulation (Section 4.2.1): tests increasing the number of source categories from 5 to 14 (Figure S4).
- New Section 4.3.1 regional case studies: Indo-Gangetic Plain, tropical wetlands (Congo Basin, Amazon, Borneo), Caspian region.
- New Section S4 in the Supplement: model–observation comparison including globally averaged time series (Figure S11) and inter-hemispheric gradient diagnostics (Figure S12).
- Substantial revisions to Section 4.1.4 (Comparison with previous datasets): three categories of systematic biases explicitly identified and discussed.
- Substantial revisions to Section 4.2.3 (Atmospheric chemistry): expanded OH-KIE discussion with laboratory constraints, Fujita et al. (2020) leverage analysis, and inversion implications; new dedicated paragraph on Cl and soil sinks.
- Restructured Section 4.3 (Discussion): split into 4.3.1 Key drivers, 4.3.2 Inversion implications, 4.3.3 Pathways for improvement.
- End-of-section summaries added throughout Sections 4.1 and 4.2.
- Quantitative satellite detectability discussion in the Conclusions.